J Mater Sci (2007) 42:3651–3660
DOI 10.1007/s10853-006-1349-0

The effect of Ti^{4+} ions and gamma radiation on the structure and electrical properties of Mg ferrite

M. A. Ahmed · E. Ateia · F. M. Salem

Received: 21 April 2005 / Accepted: 3 March 2006 / Published online: 30 January 2007

Abstract Ferrite samples of the general formula $Mg_{1+x}Ti_xEr_yFe_{2-2x-y}O_4$; $0.1 \le x \le 0.9$, $y = 0.025$ were prepared using the standard ceramic method. The final sintering temperature was 1,200 °C with heating rate 4 °C/min during 100 h. X-ray diffraction analysis was carried out to assure the formation of the spinel structure. The effect of Ti^{4+} ion concentration on the structural and the electrical properties of the investigated samples is studied. It change the iron ion concentration from 2 to $2–2x$ thereby decreasing the number of ferrous ions on octahedral sites, with a consequent decrease the dielectric constant. The most important result of γ-irradiation on the electrical properties is the change of ratio Fe^{2+}/Fe^{3+} on the octahedral site leading to increase the conductivity as well as the dielectric constant. The variation of the thermoelectric power with a temperature is performed, the common feature of all compositions is the fluctuation of Seebeck coefficient between positive and negative over the whole range of temperature. This indicates that the charge carriers are electrons and holes, depending on both the temperature range and the additive in the ferrite samples.

Introduction

It is well known that spinel ferrites play an important role in the technological applications because of their remarkable electrical and magnetic properties particularly in radio frequency region, physical flexibility, high electrical resistivity, mechanical hardness and chemical stability [1].

El Hiti [2] studied the effect of temperature, frequency and composition on the dielectric behavior and ac electrical conductivity for a series of Zn-substituted Ni–Mg ferrite samples. All samples were prepared using the usual ceramic technique. The experimental results indicated that, the real dielectric constant ε', dielectric loss $\tan\delta$ and real ac electrical conductivity σ increase with increasing temperature. The activation energy E_f for electric conduction in the ferromagnetic region, ε' and $\tan\delta$ decrease while the ac conductivity $\sigma_2(\omega)$ increases as the frequency increases. ε' has high values and $\tan\delta$ shows dielectric relaxation processes at relatively higher temperatures. The relaxation frequency f_D shifts to higher values as the temperature increases. σ, $\tan\delta$, and ε' increase while the Curie temperature T_c and the activation energy for electric conduction decreases as Zn ion substitution increases.

Mazen and Mansour [3] studied some physical properties (such as lattice parameter, density and porosity) and magnetic properties of the system $Mg_{1-x}Zn_xFe_2O_4$; where $x = 0$, 0.1, 0.2, 0.3, 0.4, 0.5 and 0.6. It was found that the lattice parameter increases with increasing the zinc concentration. The composition dependence of the physical properties is divided into two regions. The first one is for $x \le 0.3$ and the second one is for $x > 0.3$. From the magnetization measurements, the basic composition of ($MgFe_2O_4$) shows the lowest magnetization, while the composition of $x = 0.4$ shows the highest one. The behavior of magnetization M versus composition shows also two regions for

M. A. Ahmed · E. Ateia (✉) · F. M. Salem
Physics Department, Faculty of Science, Cairo University, Giza, Egypt
e-mail: drebtesam2000@yahoo.com

$x <> 0.3$. The behavior of M versus x was discussed in the basis of cation distribution. The Curie temperature T_C was determined from the measurements of the initial permeability μ_i versus temperature. It was found T_C decreases with increasing Zn-content. Also paramagnetic temperature T_P was determined from the behavior of M_S versus T. In general it was found $T_P > T_C$ by about 7–10 K.

Elementary charged particles and electromagnetic radiation with high energy interact with electronic shells or the atomic nuclei of substances passing through them. These interactions result in an elastic and inelastic scattering of particles attended by the excitation and ionization of the atoms, as well as the nuclear reactions and also disturbances in the structure of the matter, so called radiation damage [4]. In certain materials a permanent change in electrical properties could be produced by radiation damage to the crystal. This change in properties can be measured as a function of the absorbed dose in the detector, so the system then becomes an integrating dosimeter. The proposed fusion reactors designs require structural and electrical materials that will work satisfactorily after exposure to energetic ionizing radiation at high temperatures. Ferrites are being considered to be suitable for these applications [5]. Mg–Ti rare earth ferrite is one of the most important spinel ferrites due to its wide range of applications. From this outstanding point we intended to study the properties of Mg–Ti ferrite and tried to improve its electrical properties by varying many parameters such as ion substitutions, and irradiation doses to obtain well applicable ferrites.

Experimental procedure

The rare earth ferrite samples were prepared by usual standard ceramic technique [6] using analar grade oxides (BDH). The pre sintering was done at 900 °C for 15 h using lenton furnace type UAF 16/5 (England). The samples were compressed into pellet form using hydraulic press with pressure of 5×10^8 N/m^2. The final sintering was carried out at 1,200 °C for 100 h and then cooled to room temperature with the same rate of heating (4 °C/min). The pellets were well polished, and the two surfaces of each pellet were coated with silver paste and checked for a good conduction. The real part of the dielectric constant (ε') and ac conductivity (σ) were measured using a self-calibrated Hioki RLC Hi tester type 3530 (Japan) as a function of temperature from 300 to 750 K at frequencies ranging from 100 kHz to 5 MHz. The bridge automatically collects the data using a specially designed Lab view based software. The data was saved in text format that can be reported easily with Excel. The sample was inserted between the two cell electrodes. A non inductive and calibrated furnace was used for heating the samples with constant rate. The temperature of the samples was measured using a K-type thermocouple connected to a Digi-Sense thermometer (USA) with junction in contact with the sample. The accuracy in measuring temperature was better than ±1 °C.

X-ray diffraction patterns were carried by Diano X-ray diffractometer with CoK_α radiation to ensure the formation of the sample structures. The samples were irradiated with γ-ray (10, 20,and 30 Mrad). The irradiation was carried out at the National Center of Radiation Technology, Cairo, Egypt by using a gamma cell 4000. Irradiation facility (manufactured at Bhabha Atomic Research Center, India).

Results and discussion

Figure 1 shows the X-ray diffractograms for $Mg_{1+x}Ti_x$-$Er_yFe_{2-2x-y}O_4$; $x = 0.0$, 0.5, $y = 0.0$ and $x = 0.5$, $y = 0.025$. The diffraction patterns show that the samples with $x = 0, 0.5$, and $y = 0$ posses the spinel structure, while some extra phases appear for the sample with $x = 0.5$, and $y = 0.025$. This can be attributed to the large ionic radius of E^{3+} ion to occupy the tetrahedral and octahedral sites [7].

The effect of Ti^{4+}ion concentration on the structure of $Mg_{1+x}Ti_xEr_yFe_{2-2x-y}O_4$; $y = 0.025$ and $0.3 \le x \le 0.9$ is shown in Fig. 2. All investigated samples are sintered at temperature 1,200 °C with a heating rate of 4 °C/min during 100 h. The diffraction patterns show that all samples posses the spinel structure with the appearance of small peaks designated as a secondary phases. The interplaner distance "d" of the corresponding planes increases evidently at the initial substitution of Ti from $x = 0.3$ to 0.9. This is an indication to the increase of the unit cell dimensions. In other words when octahedral B site is diluted by Ti according to the Monte Carlo Simulation of Scholl and Binder [8], the lattice parameter increases as shown in Fig. 3. The increase in the lattice parameter is due to the replacement of Fe^{3+}(0.645 Å) ions by Ti^{4+}(0.605 Å) and Mg^{2+} (0.72 Å) ions [9]. The correlation between the ionic radii and the theoretical lattice constant (a_{th}) is calculated [6] using the Eq. 1

$$a_{th} = \frac{8}{3\sqrt{3}}[(r_A + R_o) + \sqrt{3}\,(r_B + R_o)] \quad (1)$$

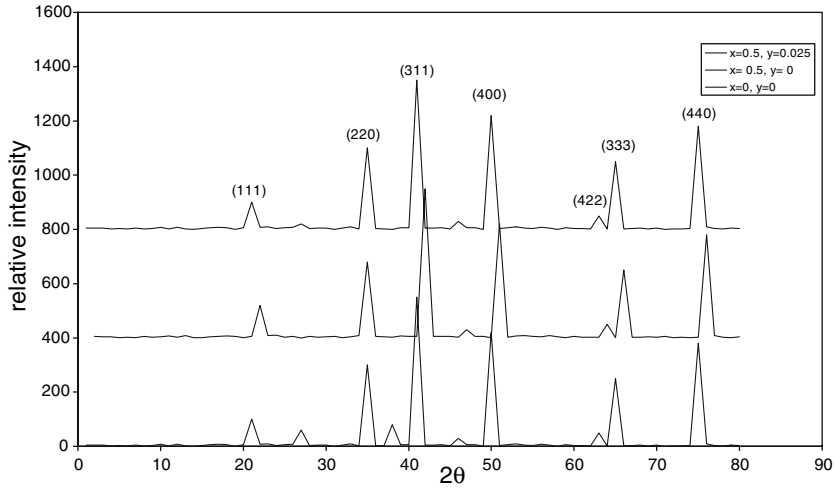

Fig. 1 X-ray diffractograms for $Mg_{1+x}Ti_xEr_yFe_{2-2x-y}O_4$; $x = 0.0$, 0.5 for $y = 0.0$, and $x = 0.5$ for $y = 0.025$

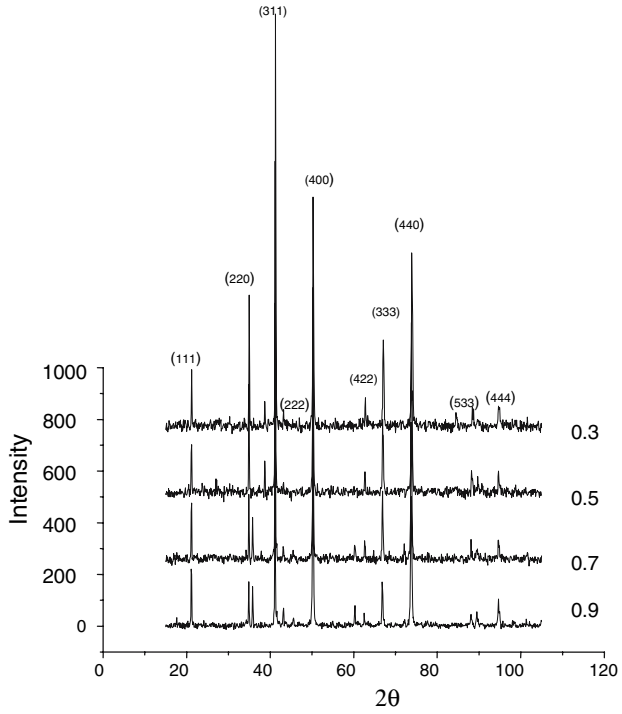

Fig. 2 X-ray diffractrogram for $Mg_{1+x}Ti_xEr_yFe_{2-2x-y}O_4$; $0.3 \leq x \leq 0.9$, $y = 0.025$ sintered at 1,200 °C with heating rate of 4 °C/min

where R_o is the radius of the oxygen ion (0.138 nm) [10], r_A and r_B are the ionic radii of tetrahedral (A) and octahedral (B) sites, respectively. In order to calculate r_A and r_B it is necessary to know the cation distribution for a given system. In general, Ti^{4+} ions have higher preference for B-sites while Mg^{2+} and Fe^{3+} ions are distributed between the tetrahedral (A) and octahedral (B) sites, so the formula of the cation distribution can be written as

$$(Fe^{3+}_{1-x}Mg^{2+}_{x})[Fe^{3+}_{1+x-2t}Mg^{2+}_{1+t-x}Ti^{4+}_{t}]O_4 \quad (1)$$

where the brackets () and [ ] indicate A and B sites respectively. The ionic radii of the tetrahedral r_A and octahedral r_B against Ti^{4+} ion concentration (x) are reported in Table 1.

The obtained data shows that r_A increases and r_B decreases with increasing x, this is because increasing Ti^{4+} ions, will associated with the replacement of $2x$ of Fe^{3+} (0.645 Å) by x of Mg^{2+} ions and x of Ti^{4+} ions according to the representative formula of this ferrite while tetrahedral Fe^{3+}(0.4900 Å) ions are mainly released by Mg^{2+} ions. This process will be taken into account that the ratio of Mg^{2+} ions in tetrahedral is higher than in octahedral site.

The oxygen positional parameter (u) depends on the chemical composition, preparation conditions and heating procedure [11], it is given by the following relation [12, 13]

$$u = \left[(r_A + R_o)\frac{1}{\sqrt{3}a} + \frac{1}{4}\right] \quad (2)$$

where (a) is the lattice constant. The theoretical and the experimental values of the lattice parameter and oxygen positional parameters of the investigated samples are reported against Ti concentration (x) in Table 2. The oxygen positional parameter (u) for all spinel ferrite, has a value near (0.375 Å) [14]. For the investigated samples, (u) is of order (0.3820 Å), which indicates the presence of some deviations from the case of spinel ferrite due to the difference in the preparation conditions[12]. The difference between $a_{exp.}$ and $a_{th.}$ may be related to the lattice defects for polycrystalline material and the presence of Fe^{2+} ions on A or B sites

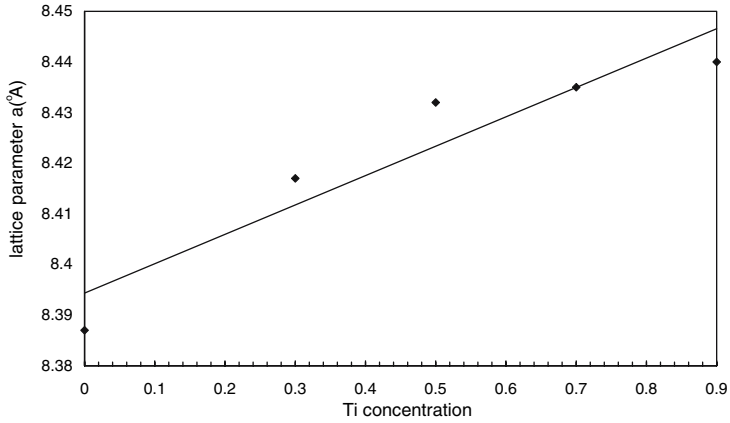

Fig. 3 The variation of the lattice parameter a (°A) as a function of Ti concentration for $Mg_{1+x}Ti_xEr_yFe_{2-2x-y}O_4$; $0 \leq x \leq 0.9$ $y = 0.025$, sintered at 1,200 °C, reached with a heating rate of 4 °C/min

Table 1 Values of r_A and r_B as a function of Ti ion concentration (x)

Sample	r_A (Å)	r_B(Å)
$Mg_{1.3}Ti_{0.3}Er_{0.025}Fe_{1.375}O_4$	0.514	0.676
$Mg_{1.5}Ti_{0.5}Er_{0.025}Fe_{0.975}O_4$	0.530	0.672
$Mg_{1.7}Ti_{0.7}Er_{0.025}Fe_{0.575}O_4$	0.546	0.668
$Mg_{1.9}Ti_{0.9}Er_{0.025}Fe_{0.175}O_4$	0.562	0.664

Table 2 Values of $a_{exp.}$ $a_{th.}$ and $u_{exp.}$, u_{th} at $y = 0.025$ as a function of Ti content (x)

Ti (x)	$a_{exp.}$(Å)	$a_{th.}$(Å)	$u_{exp.}$(Å)	u_{th}(Å)
0.3	8.417	8.396	0.3799	0.3800
0.5	8.432	8.410	0.3800	0.3810
0.7	8.435	8.424	0.3810	0.3820
0.9	8.440	8.438	0.3828	0.3828

which are not taken into account [15]. The observed linear increase of lattice constant can be attributed to the difference in ionic radii as mentioned before.

The porosity of the samples is calculated using the relation $P = 1–D/D_x$ [13]. X-ray density (D_x) is calculated from the relation [16]

$$D_x = \frac{ZM}{NV} \tag{3}$$

where Z is the number of molecules per unit cell ($Z = 8$), M is the molecular weight, N is Avogadro's number; and V is the unit cell volume (lattice parameter). The bulk density (D) is determined by using Archimedes principal in the toluene according to the following formula

$$D\frac{W_s}{W_t}\rho_t \tag{4}$$

where W_s denote the mass of the specimen in air, W_t is the apparent loss in toluene, and ρ_t is the density of toluene.

The variation of bulk density (D), X-ray density (D_x) and the porosity (P) as a function of Ti concentration (x) are tabulated in Table 3. The data show that the porosity nearly increases with increasing Ti content. this can be attributed to Ti^{4+} ions with relatively smaller radius replace the Fe^{3+} ions on octahedral site, initiate some vacancies with the result of increasing porosity of the sample[17]. Both D and D_x decrease with increasing Ti content i.e. the bulk density nearly reflects the same general behavior of the X-ray density.

Figure 4 is a set of typical curves indicating the variation of the real part of the dielectric constant ε′ with the absolute temperature for $Mg_{1+x}Ti_xEr_yFe_{2-2x-y}O_4$; $y = 0.025$ and $0.1 \leq x \leq 0.9$, at the applied frequencies (50 kHz–1 MHz) with sintering temperature of 1,200 °C and heating rate of 4 °C/min, respectively. The figure shows clearly that ε′ is increased slowly with temperature up to $T \approx 500$ K followed by a large increase passing through the transition temperature of each sample. This may be due to the following: the small thermal energy given to the system is not sufficient enough to free the localized dipoles and to orient them in the field direction. In this region, ε′ is nearly temperature independent which means that the electronic polarization is the most predominant one. In the second region of temperature ε′ is increased for all samples but with different rates depending on Ti concentration. This increase is due to electron hopping

Table 3 Values of D, D_x and P as a function of Ti^{4+} ion concentration

Ti (x)	Bulk density D (g/cm^3)	X-ray density D_x (g/cm^3)	Porosity (P)
0.3	3.890	4.252	0.0851
0.5	3.325	4.054	0.1798
0.7	3.235	3.884	0.1671
0.9	2.637	3.696	0.2865

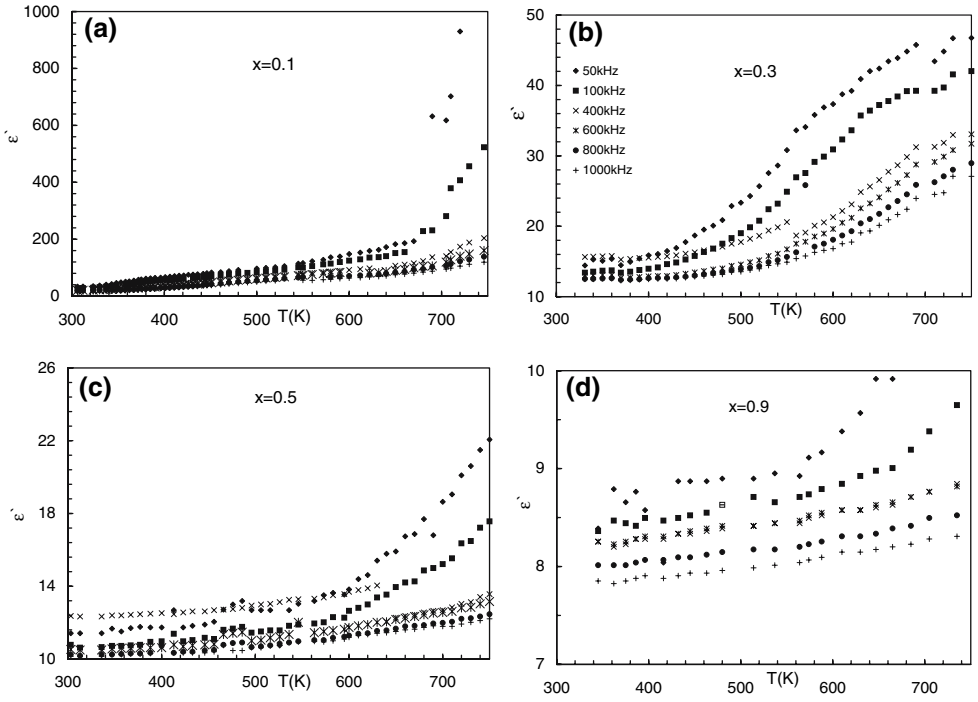

Fig. 4 (**a–d**) The variation of the real part of the dielectric constant (ε′) with the absolute temperature T(K) at different frequencies for $Mg_{1+x}Ti_xEr_yFe_{2-2x-y}O_4$; $0.1 \leq x \leq 0.9$, y=0.025, sintered at 1,200 °C, reached with heating rate 4 °C/min

between the ferrous and ferric ions on the octahedral sites. This electron hopping causes local displacement in the external field direction, producing change of polarization as well as of ε′ [18]. The decrease in ε′ with increasing frequency is due to the fast alternation of the electric field accompanied with the applied frequency, where the alternation of the dipoles increases as well as the friction between them. The quantity of heat dissipated in the entire volume of the sample increases and the aligned dipoles will be disturbed with the result of decreasing ε′.

The variation of the dielectric constant (ε′) with frequency for the above investigated samples is shown in Fig. 5. The samples revealed dispersion due to Maxwell–Wagner interfacial polarization [19, 20], which is of good agreement with Koops phenomenological theory [21]. The data shows that the dispersion of dielectric constant with frequency is maximum for the sample with $x = 0.1$. A comparison of the dispersion curves for the samples with increasing Ti ion concentration shows that, the change in the value of the dielectric constant at lower frequencies is larger than that at higher frequency of the externally applied field. In other words the electronic exchange between ferrous and ferric ions can not follow the alternating field [22] leading to a decrease in the dielectric constant (ε′). The observed variation in the dielectric relaxation intensity can be explained on the basis of space charge polarization due to the inhomogeneous dielectric structure of the samples [19]. The effective number of ferrous ions on octahedral sites available for electric polarization decreases with increasing Ti concentration, with the result of decreasing of the dielectric relaxation intensity.

Figure 6 is a typical curve, correlates the ac conductivity ln (σ) and the reciprocal of absolute

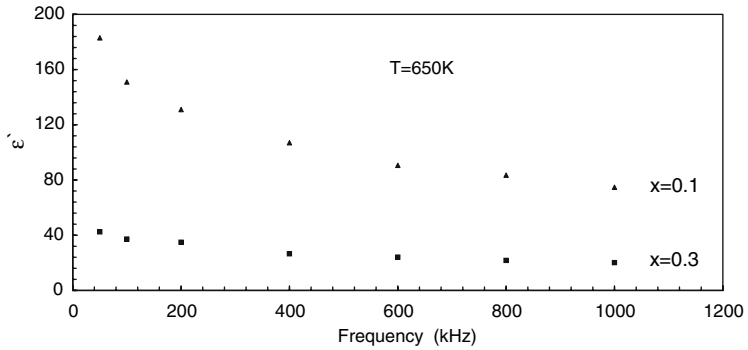

Fig. 5 Dependance of the real part of the dielectric constant (ε′) on the frequency for $Mg_{1+x}Ti_xEr_yFe_{2-2x-y}O_4$; y = 0.025 at fixed temperature T = 650 K

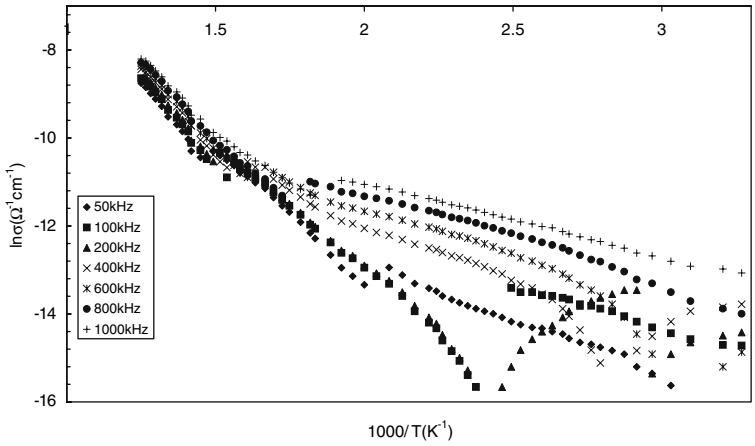

Fig. 6 Dependence of the ac conductivity ln (σ) on the reciprocal of the absolute temperature (1,000/T)(K–1) at different frequencies for $Mg_{1+x}Ti_xEr_{0.025}Fe_{2-2x-y}O_4$4, x = 0.1, sintered at 1,200 °C, with heating rate of 4 °C/min

temperature at different frequencies for the sample with $x = 0.1$, $y = 0.025$ sintered at 1,200 °C with a heating rate of 4 °C/min. From the figure it is clearly that the data obeys the well known Arrhenius relation [23] $\sigma = \sigma_o \exp(-E/kT)$, where σ_o is a constant, k, E and T are the Boltzmann's constant, activation energy and the absolute temperature, respectively. Increasing temperature leads to an increase in σ, which is the normal behavior of semiconducting material. Two conduction mechanisms are expected here, the first one below the transition temperature where the conductivity is frequency and temperature dependent [24]. While the second mechanism above the transition temperature which is; temperature dependent and frequency independent, is related to the drift mobility of the electric charge carriers. On passing through the transition temperature, a change in the gradient of the straight line takes place. The magnitude of this gradient depends on the exchange interaction between the outer and inner electrons of the metal ions, which is changed at the transition temperature due to transfer of the system from the ferrimagnetic (ordered) to the paramagnetic (disordered) state. Increasing the temperature of the sample will help the trapped charges to be liberated and participate in the conduction process, with the result of increasing the conductivity. This increase in σ could be related to the increase in the drift mobility of the thermally activated electrons according to the hopping conduction mechanism and not to thermally creation of the charge carriers. The valence exchange $Fe^{2+} \leftrightarrow Fe^{3+} + e^-$ is the main source of electron hopping in this process. Nearly the same trend is observed for all Ti^{4+} ion concentration.

Table 4 shows the activation energies of low (E_I) and high (E_{II}) temperature regions at different Ti concentration (x) for the investigated samples. The obtained data of (E_I) and (E_{II}) shows that the activation energy for electric conduction in the paramagnetic region (E_{II}) is higher than that in the ferrimagnetic region (E_I). This could be related to the disordered state in the paramagnetic region with respect to the ordered one in the ferrimagnetic region. This result is in agreement with the theory developed by Irkhin and Turov [25]. Ti^{4+} ion concentration act as scattering center for the charge carriers hence the conductivity decreases and the activation energy increases [26].

Table 4 The activation energy in eV for the low (E_I) and high (E_{II}) temperature regions at different Ti concentration

Ti (x)	100 kHz		1,000 kHz	
	E_I (eV)	E_{II} (eV)	E_I (eV)	E_{II} (eV)
0.1	0.172	0.516	0.086	0.344
0.3	0.501	0.5375	0.3225	0.430
0.5	0.516	0.688	–	0.602
0.7	–	–	–	0.860

Figure 7 shows the compositional dependence of (ε', ε'' and σ) at the selected frequency and temperature for $Mg_{1+x}Ti_xEr_yFe_{2-2x-y}O_4$; at the same preparation conditions. As shown from the figure (ε') has the same trend as the conductivity (σ) [21] which confirms the assumption that the mechanisms of the conductivity and the dielectric constant are of the same origin. The data of (ε', ε'' and σ) decrease with increasing Ti^{4+} ion concentration and become nearly constant at higher Ti concentration. This result is explained in view of the hopping conduction mechanism between $Fe^{2+} \leftrightarrow Fe^{3+} + e^-$, Ti^{4+} ion does not participate in conduction process but limit the degree of hopping by blocking up $Fe^{2+} \leftrightarrow Fe^{3+} + e^-$ pattern on the B sites [27]. Increasing Ti^{4+} ion concentration reduce the net Fe^{3+} ion concentration by $2x$. This reduces the ratio Fe^{3+}/Fe^{2+} available for conduction.

Figure 8 shows X-ray diffractograms for $Mg_{1.1}Ti_{0.1}Er_{0.025}Fe_{1.775}O_4$; before and after irradiation

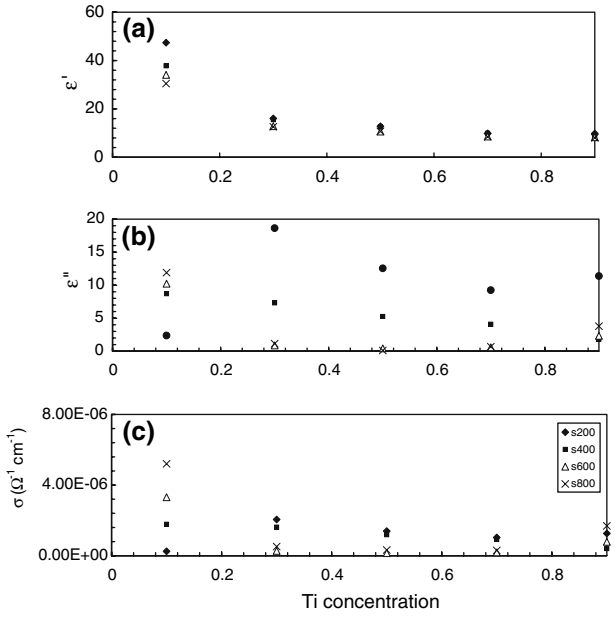

Fig. 7 (**a–c**) Dependence of ε′, ε′′ and σ on Ti concentration (x) at certain absolute temperature 400 K, and different frequencies

with γ-rays sintered at 1,200 °C using heating rate of 4 °C/min. From the figure, a noticeable shift for the peaks occurred.

In other words the observed effects depend on the mechanism of interaction of irradiating wave with the ions of the material with context to the structure, the γ-radiation may change the ratio of Fe^{2+}/Fe^{3+} on the octahedral sites as a consequence of $\gamma + Fe^{2+} \leftrightarrow Fe^{3+} + e^{-}$, which leads to a change in the crystal size [5]. Table 5 reports the variation of the interplaner distance, relative intensity and Miller indices for the irradiated and unirradiated sample. The observed interplaner distance (d) of the corresponding planes decreases with radiation doses. This result agrees well with our expectation.

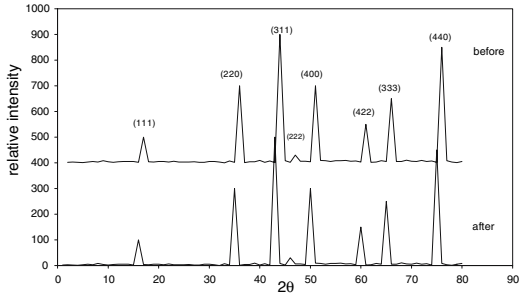

Fig. 8 X-ray diffractogram for $Mg_{1+x}Ti_xEr_yFe_{2-2x-y}O_4$; $x = 0.1$, $y = 0.025$ sintered at 1,200 °C with heating rate 4 °C/min, before and after 30 Mrad

Table 5 Values of d spacing, relative intensity I/I_o and Miller indices (hkl) for irradiated and unirradiated $Mg_{1.1}Ti_{0.1}Er_{0.025}Fe_{1.775}O_4$

Before irradiation			After irradiation by 30 Mrad		
dÅ	I/I_o	hkl	dÅ	I/I_o	hkl
4.880	6.10	111	4.866	8.10	111
2.980	10.30	220	2.950	51.00	220
2.530	100.00	311	2.520	100.00	311
2.067	47.00	400	2.090	25.50	400
1.710	11.29	422	1.700	13.21	422
1.617	29.67	511	1.610	44.10	511
1.480	59.64	440	1.480	65.86	440
System: spinel			System: spinel		
a = 8.3842 Å			a = 8.350 Å		
V = 589.383 Å^3			V = 582.272 Å^3		

Figure 9 shows the variation of ε′, with the absolute temperature as a function of frequency for the investigated samples, $x = 0.1$ at different doses of 0.0, 10, 20 and 30 Mrad. The data in the figure gives the same trend, as described before, with the appearance of small humps in the irradiated samples. This can be explained in a view of interaction of γ-rays with the matter, which is summarized in two steps. The first one is the increase in hopping rate caused from depressing the jump length with the result of more interaction between Fe^{3+} and Fe^{2+}. These jumping electrons oriented in the field direction and consequently giving rise to ε′ where the production of Fe^{2+} after irradiation was confirmed by Mousa et al. [28]. The second step is the generation of some vacancies at different depths which act as trapping centers. The liberation of charge carriers from these trapping centers needs different energies. In Fig. 9c, 20 Mrad γ-rays is not the sufficient energy to liberate charge carriers from the trapping centers at deeper depths, leading to a decrease in ε′. Figure 9d shows a drastic increase in ε′ which can be explained in view of the structural changes due high γ-doses. All the above processes are summarized in Fig. 9e which is taken at a constant temperature $T = 500$ K, and $f = 100$ kHz. In other words the four oxygen anions surrounding the metal ions in tetrahedral sites are displaced outwards along the body diagonal of the cube. These four oxygen anions still occupy the centers of an enlarged tetrahedron and retain the cubic symmetry [29]. Some distortion occurs to the tetrahedral sites due to such displacement and it will move the anions away from the nearest tetrahedral cations. The result of this process is an increase in the polarization as well as the rate of the electron exchange between ferrous and ferric ions in the high resistivity region.

Figure 10 correlates the variation of the electrical conductivity ln σ with the reciprocal of absolute

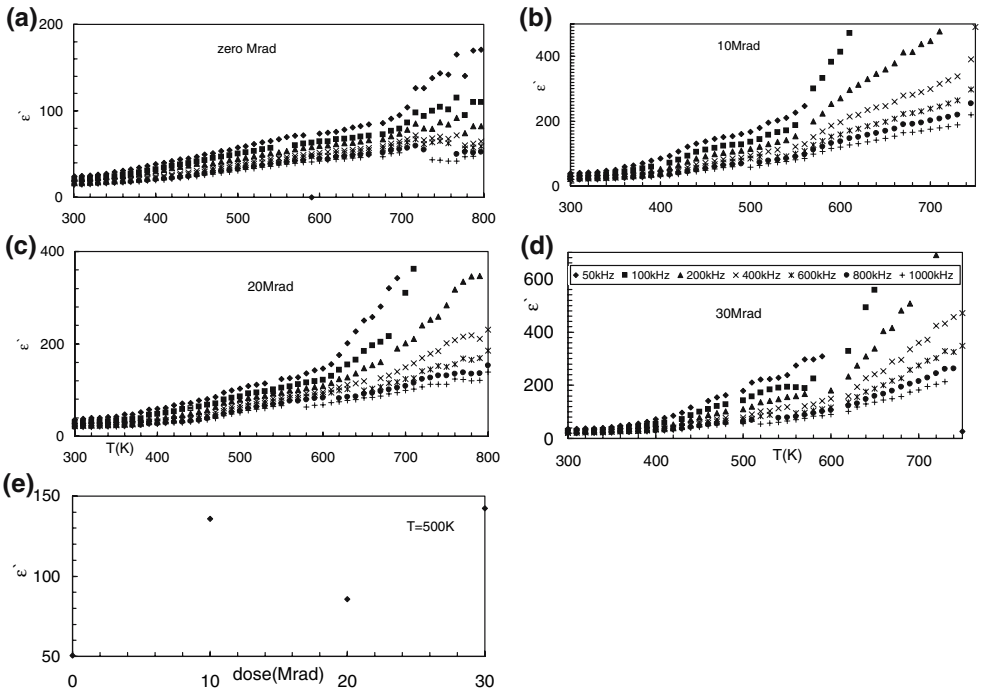

Fig. 9 (**a–e**) The variation of the real part of the dielectric constant (ε′) with the absolute temperature at different frequencies for $Mg_{1+x}Ti_xEr_yFe_{2-2x-y}O_4$; $x = 0.1$, $y = 0.025$ before and after irradiation by γ-rays of different doses Fig. 9**e**. The variation of the real part of the dielectric constant ε′ with different doses at $T = 500$ K, and $f = 100$ kHz

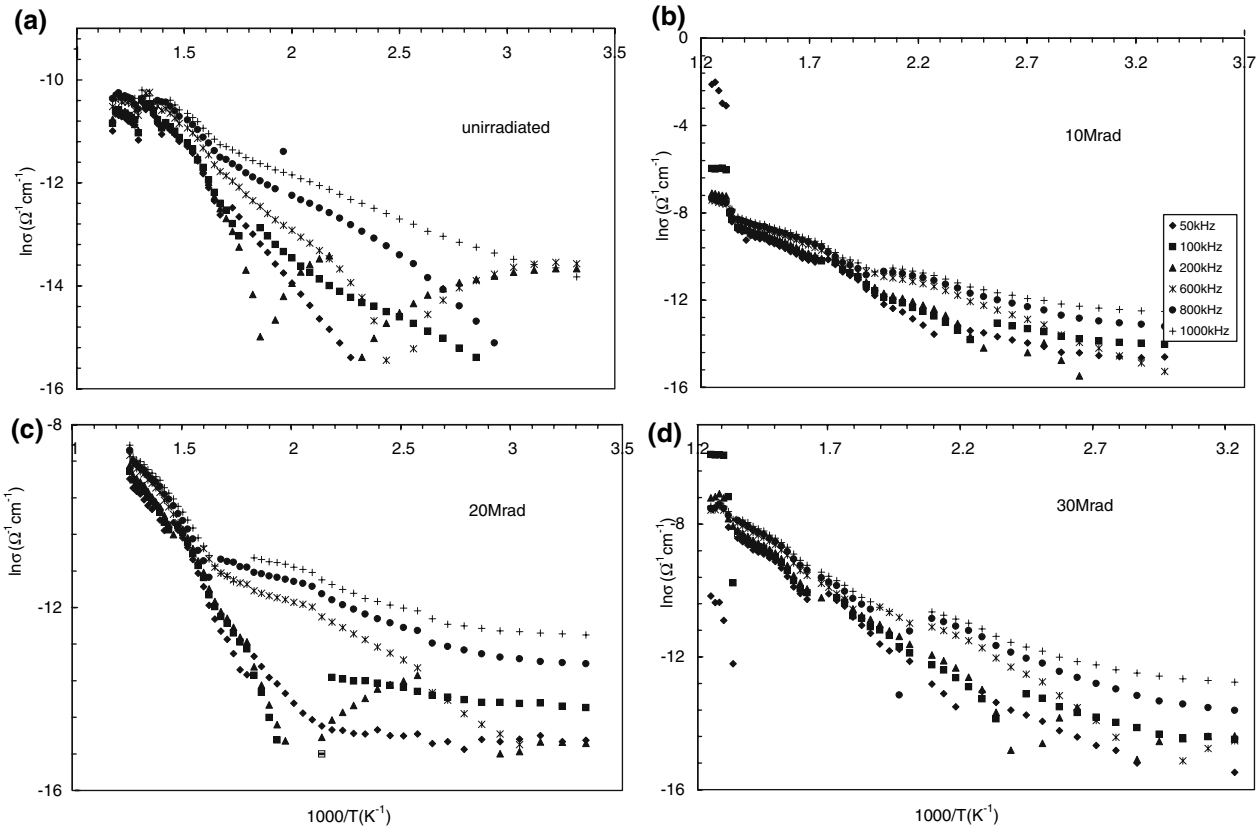

Fig. 10 (**a–d**) The variation of the ac conductivity (ln σ) with the reciprocal of the absolute temperature (1,000/T)(K–1) for $Mg_{1+x}Ti_xEr_yFe_{2-2x-y}O_4$; $x = 0.1$, $y = 0.025$ before and after irradiation with different doses of γ-rays

temperature as a function of the applied frequency before and after γ-irradiation. From the figure it is clear that, the conductivity increases as the γ-dose increases even in the case of 20 Mrad which still has higher conductivity values than the unirradiated samples. This increase in σ can be attributed to the increase

in the ratio of Fe^{2+}/Fe^{3+} on the octahedral sites as a consequence of the hopping reaction [30]. By comparing the transition temperature of the investigated sample irradiated at (0, 10, 20 and 30 Mrad) one can find that, the transition temperature increases with increasing dose as a result of increasing the ordered region.

In other words, the arrangement of the magnetic dipoles takes place due to effect of the energy of γ-radiation on the expense of paramagnetic region, though increasing T_c [31]. The values of the activation energy decrease with increasing dose and the data are reported in Table 6.

Figure 11 illustrates the variation of thermoelectric power (s) with temperature for the investigated samples. As shown from the figure the common features of all composition are the fluctuation of Seebeck coefficient between positive and negative over the whole range of temperature indicating that the charge carriers are both electrons and holes. The values of Seebeck coefficient are positive for lower Ti concentration. This positivity decreases with increasing Ti concentration until nearly vanish at $x = 0.9$. The increase in the Seebeck coefficient with temperature had been also observed in other ferrites [32]. This is due to the increase in the mobility of charge with the increasing temperature.

Table 6 The activation energy, for the low (E_I) and high (E_{II}) temperature regions at different γ-radiation doses

Dose (Mrad)	E_I (100 kHz) (eV)	E_I (1000 kHz) (eV)	E_{II} (100 kHz) (eV)	E_{II} (1,000 kHz) (eV)
0	0.286	0.172	0.737	0.344
10	0.172	0.086	0.516	0.258
20	0.114	0.0573	0.344	0.114
30	0.0573	0.043	0.258	0.086

Conclusion

1. All samples reveal spinel structure in spite of the presence of rare earth ions.
2. Both electrical conductivity and dielectric constant decrease as Ti^{4+} ion substitution increases.

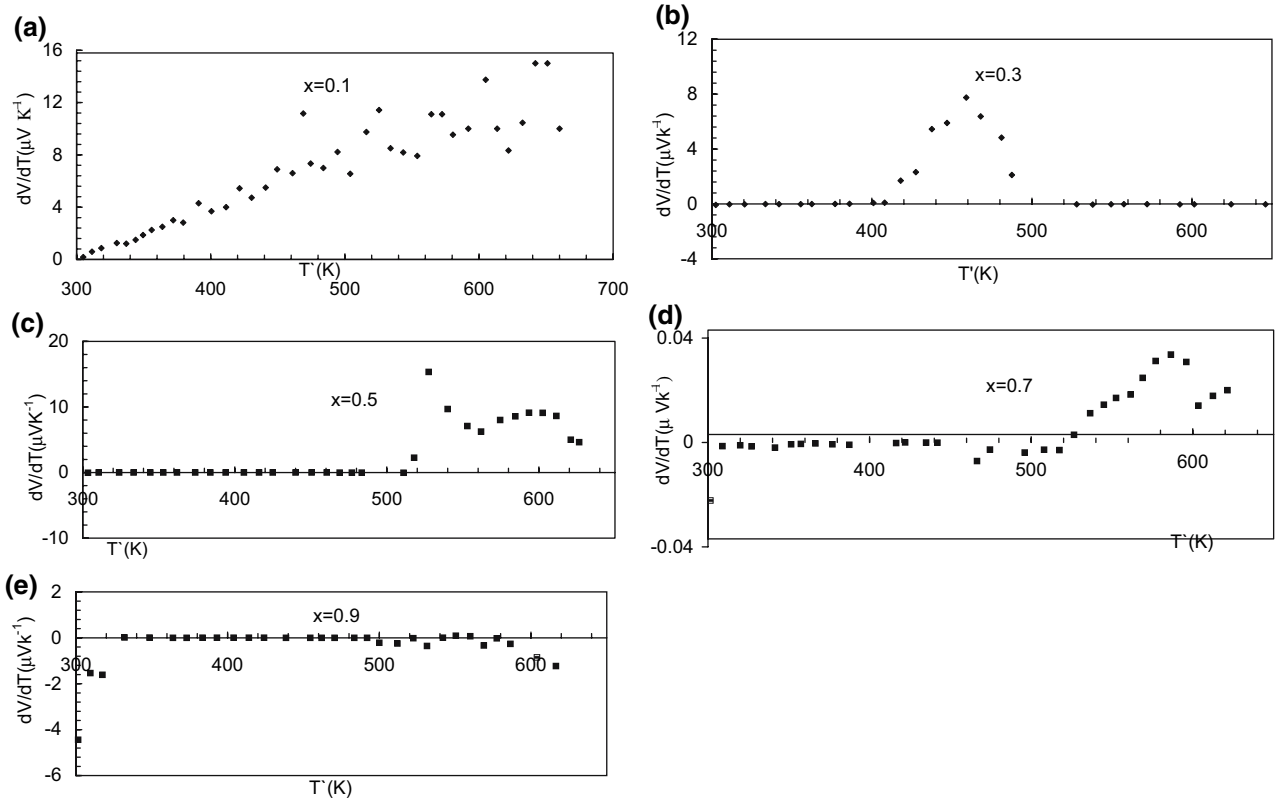

Fig. 11 (**a-e**) The variation of thermoelectric power with the absolute temperature for $Mg_{1+x}Ti_xEr_yFe_{2-2x-y}O_4$; $0.1 \le x \le 0.9$, sintered at 1,200 °C with heating rate of 4 °C/min during 100 h

3. In both irradiated and un irradiated samples the activation energy in the paramagnetic region is higher than that in the ferromagnetic region.
4. The interplaner distance of the investigated samples decreases with increasing γ-doses.

References

1. Rezlescu E, Rezlescu N, Popa PD, Pasnicu C (1997) Phys Stat Sol (a) 162:673
2. El Hiti MA (1996) J Magn Magn Mater 164:187
3. Mazen SA, Mansour SF (2003) Cryst Res Technol 38(6):471
4. Tareev B (1979) Physics of dielectric materials. Mir Publishers, Moscow
5. Darwish NZ, Hemeda OM, Abd El-Ati MI (1994) Appl Radiat Isot 45(4):445
6. Valenzuela R (1994) Magnetic ceramics, Cambridge University Press.
7. Rezlescu N, Rezlescu E, Pasnicu C, Craus ML (1994) J Phys Condens Matter 6:5707
8. Scholl F, Binder K (1980) Z Physiother B39:239
9. Shanon RD (1976) Acta Crystallogr A32:751
10. Vasiliu A, Maxim Gh, Craus ML, Luca E (1972) Phy Stat Sol A 13:371
11. Khan Y, Kneller E (1978) J Magn Mater 7:4
12. Vijaya Kumar K, Ravinder D (2001) Int J Inorg Mater 3:661
13. Standley KJ (1972) Oxide magnetic materials. Clarendon Press, Oxford
14. Verwey EJW, Heilmann EL Jr (1947) Chem Phys 15:174
15. Potalova A, Dzueru N, Romanov UP (1972) Phys Stat Sol (a) 12:623
16. Ahmed MA (1989) Phys Stat Sol (a) 111:567
17. Purushotham Y, Reddy VD, Sagar DR, Kishan P, Reddy PV (1993) Phys Stat Sol (a) 140:k89
18. Vengopal Reddy P, Rao TS (1982) J Less Common Met 86:255
19. Maxwell JC (1929) Electricity and Magnetism, vol 1. Oxford University Press, Oxford (Section 328)
20. Wagner KW (1913) Ann Phys Leipzig 40:817
21. Koops CG (1951) Phys Rev 83:121
22. Iwauchi K (1971) Jpn J Appl Phys 10:1520
23. Smit J, Wijn HPJ (1959) Ferrites, Joan Wiley and Sons Publishing, New York
24. Abdeen AM (1998) J Magn Magn Mater 185:199
25. Irkhin Y, Turov EA (1957) Sov Phys JETP 33:673
26. Mazen SA (2000) Mater Chem Phys 62:131–138
27. Mirebeau I, Iancu G, Hennion M, Gaviolle G, Hubsch J (1996) Phys Rev B Condens Matter (USA) 54:22
28. Mousa MA, Summan AM, Ahmed MA (1989) Thermochim Acta 144:45
29. Murthy VKR, Sobanadri J (1976) Phys Stat Sol (a) 36:133
30. Ahmed MA, Mohsen F (1997) Egypt J Phys 1:151
31. Hemeda OM, Darwish NZ (1994) Appl Phys Commun 13(1):29
32. Patil SA, Patil BL, Sawant SR (1993) Ind J Pure Appl Phys 31:904